ASSESSMENT OF REDUCED-KINETICS MECHANISMS FOR COMBUSTION OF JET FUEL IN CFD APPLICATIONS

Kumud Ajmani
Vantage Partners, LLC
Cleveland, OH, USA

Krishna P. Kundu
NASA Glenn Research Center
Cleveland, OH, USA

Shaye J. Yungster
Ohio Aerospace Institute
Cleveland, OH, USA

ABSTRACT

A computational effort was undertaken to analyze the details of fluid flow in Lean-Direct Injection (LDI) combustors for next-generation LDI design. The National Combustor Code (NCC) was used to perform reacting flow computations on single-element LDI injector configurations. The feasibility of using a reduced chemical-kinetics approach, which optimizes the reaction rates and species to model the emissions characteristics typical of lean-burning gas-turbine combustors, was assessed. The assessments were performed with Reynolds-Averaged Navier-Stokes (RANS) and Time-Filtered Navier Stokes (TFNS) time-integration, with a Lagrangian spray model with the NCC code. The NCC predictions for EINOx and combustor exit temperature were compared with experimental data for two different single-element LDI injector configurations, with 60^o and 45^o axially swept swirler vanes. The effects of turbulence-chemistry interaction on the predicted flow in a typical LDI combustor were studied with detailed comparisons of NCC TFNS with experimental data.

1.0 INTRODUCTION

Next-generation emissions targets for NOx reduction set as part of NASA's N+2 Environmentally Responsible Aviation (ERA) program, have revived interest in Lean-Direct Injection (LDI) combustion devices, due to the promise shown by these combustors in N+1 development work. The LDI concept is attractive as all of the combustion air is injected directly into the combustor dome, and quick burning in relatively short zones can be easily controlled for low NOx production. Some drawbacks of LDI technology, identified in N+1 efforts, have motivated the development of innovative designs in N+2 efforts, as summarized in [Lee 2013].

The continuous nature of design evolution makes it attractive, if not essential, to use Computational Fluid Dynamics (CFD) tools to reduce the cost of injector and combustor design and testing. A CFD tool developed by NASA Glenn Research Center (GRC) for modeling of reacting flows in liquid-fueled gas-turbine combustors is the National Combustion Code (NCC). The NCC has evolved over the past twenty years as the physical models within it have been extensively assessed and validated with available experimental data. The continuous evolution of the NCC makes it very attractive as a CFD tool to help guide technology development of next generation Lean Direct Injection configurations.

The CFD analyses of [Liu, 2007] and [Iannetti, 2008] for single-element injectors have focused on using RANS and URANS computations with the NCC. More recent CFD analysis by [Liu, 2011] has extended the RANS analysis of LDI injectors to Very Large Eddy Simulation [VLES] using a Time-Filtered Navier-Stokes [TFNS] approach. More recently, [Ajmani 2013] had performed a detailed assessment of the NCC RANS for emissions predictions of single-element and multiple-element LDI-1 injectors with the reduced-kinetics mechanism of [Ajmani 2010]. The lessons learnt from the LDI-1 assessment of the NCC were applied to evaluate the performance and emissions profiles of two separate LDI-2 candidates, as reported for Woodward FST, Inc designs in [Ajmani 2014a] and United Technologies Aerospace Systems (UTAS) designs in [Ajmani 2014b].

One of the pacing aspects of any CFD analyses is the ability and accuracy to predict fuel-air mixing and attendant emissions of nitrous-oxides and unburnt hydrocarbons. Ideally, one would use a detailed chemical mechanism like GRI-Mech (100s of species, 1000s of reactions), *coupled* with the solution of the flow equations. However, this approach is computationally impracticable for CFD analysis of reacting flows in industrial geometries, where the computational mesh size may range from 10M to 100M nodes. Some CFD codes adopt the laminar flamelet approach to implement detailed chemical kinetics by using a *decoupled*, computationally inexpensive, table lookup for kinetics computations. The NCC team decided against the laminar flamelet approach because of accuracy, robustness and implementation issues for *liquid-fueled* gas turbine combustor applications. An alternative CFD approach uses simplified (one- or two-step) kinetics for heat-release computations, followed by emissions predictions in computationally inexpensive post-processing using detailed chemical kinetics ([Mongia 2008]). The efforts described in this paper assess the feasibility of using *coupled, reduced, emissions optimized* chemical-kinetics mechanisms, instead of using *decoupled* detailed mechanisms in the NCC .

The motivation for the current work is to evolve towards a "best-practice" reduced chemical kinetics mechanism for use with the NCC code, with the goal of accurately predicting emissions performance of next-generation liquid-fueled gas-turbine combustors using LDI concepts. This paper describes the implementation and assessment of a computationally feasible, *coupled,* reduced chemical-kinetics approach (10-15 species, 15-20 reaction steps) for the NCC. The *reduction* process begins with a detailed mechanism and arrives at a reduced mechanism which models the heat release and emissions characteristics (NOx, CO) trends for the flow conditions and fuel-air ratio range of interest. The NCC computations with the reduced kinetics approach were assessed for comparisons of emissions predictions with experimental data, for two different, single-element LDI-1 configurations. The CFD analysis utilized a Eulerian gas-phase model and a Lagrangian liquid-phase model, along with RANS and Time-Filtered Navier Stokes (TFNS) integration within the NCC.

2.0 REDUCED-KINETICS MECHANISM

In a previous paper [Ajmani 2010] a reduced mechanism was reported to describe the combustion of Jet-A/Air in CFD calculations. The reduced mechanism was developed mostly by comparing the ignition delays in a plug-flow reactor with published results. In aircraft gas-turbine engines, fuel is ignited by an ignitor and the initial process is similar to that in a stirred reactor; the conventional ignition delay may not be significant for CFD modeling purposes. Moreover, in LDI combustors, the fuel burns very quickly and a majority of the combustion is complete within a very short time. Hence, it may not be necessary to describe the detailed ignition reactions when modeling LDI combustor flows. In addition, it may be incorrect to assume that the combustion process attains equilibrium stage, because the measured nitrogen oxide concentrations depend on the residence time of combustion.

The physics of the LDI combustion process is somewhat between a perfectly stirred reactor and the equilibrium stage of combustion. One well-known approach to model these phenomena is to perform combustion calculations using well-stirred reaction–kinetics (WSR) in the mixing zone near the combustor face, followed by plug-flow calculations in the downstream mixed-out region. The current paper presents a kinetics mechanism that was developed using WSR kinetics, and calibrated (as necessary) to match experimental emissions data in LDI combustion calculations using the NCC. The mechanism described here assumes composition of the fuel as $C_{11}H_{21}$, which is assumed to have the same composition and thermodynamic parameters as Jet-A.

As stated above, initial complex ignition reactions are avoided in this mechanism, and the fuel molecule is assumed to break down into a hydrocarbon fragment and hydrogen atom; the hydrocarbon fragment subsequently oxidizes to carbon monoxide and carbon dioxide. The new kinetics mechanism (see Appendix A) was first developed by using WSR calculations using [Chemkin 2013], and optimizing the mechanism to match emissions characteristics of a detailed mechanism, JetSURF [Sirjean 2009]. The reduced mechanism was then assessed with a set of CFD calculations for two different LDI geometries and multiple sets of flow conditions.

2.1 COMPUTATIONAL MODELS FOR CFD

The geometry and setup configuration for the single-element test-case for the LDI computational study with the National Combustor Code (NCC) is shown in Fig 1. This configuration is referred to here as LDI-1. The setup consists of six axial swirlers (helical blade-passages with a 60° turning angle for the airflow) connected to a converging-diverging venturi, followed by the downstream combustor section. Fuel is injected at the throat of the venturi, or slightly upstream of the throat.

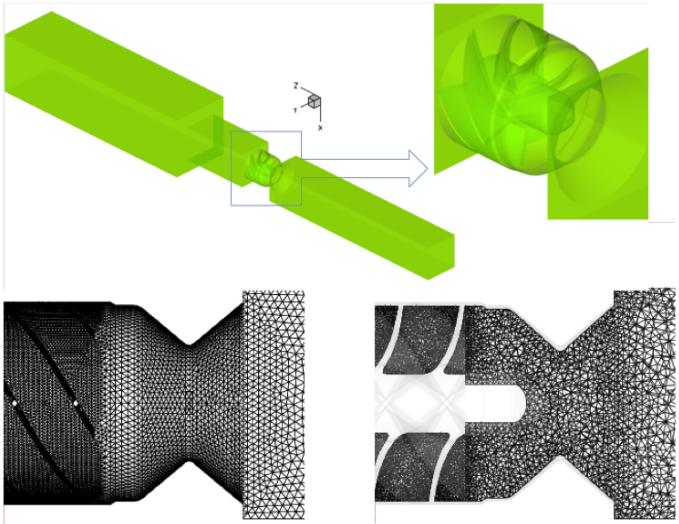

Figure 1: Computational Geometry and Tetrahedral Mesh (1.1M elements) for the single-element LDI with 60° axial-swirl helical vanes

The first step of the current computations focused on performing a detailed NCC RANS computation for a single-element LDI. Some of the best-practices from the mesh-refinement study reported in an earlier paper [Ajmani 2013] were used for this analysis. The basis of the mesh-refinement study was to obtain the best comparison with experimentally measured effective-area or pressure drop across the swirler element for non-reacting flow. Detailed comparisons were also performed between the NCC and experimental data for velocity components and turbulent kinetic-energy in the mesh-refinement study.

Second-order accurate central-differences are used for the inviscid and viscous flux discretizations, and a Jameson operator (a blend of 2nd and 4th-order dissipation terms) is used to maintain numerical stability. In order to enhance convergence acceleration in pseudo-time, implicit residual smoothing is used to smooth the computed residuals. Turbulence closure is obtained by a two-equation k-ε model with variable Cμ and generalized wall-functions with pressure-gradient effects [Shih 2003]. Steady-state RANS solutions are obtained by a four-stage, explicit Runge-Kutta integration technique.

As reported in [Ajmani 2013], several mesh configurations were studied in order to identify the best practices for meshing LDI configurations with axial bladed swirlers. The final, fully tetrahedral mesh of 1.1M elements (see figure 1) used in the current work, was obtained with the following criteria:

1. Ensure that each swirler passage has identical mesh representation.

2. Ensure that the entry region of each swirler has a high density of mesh points to account for entrance effects. This is critical to computing the correct pressure-drop through the swirler array.

3. Ensure that the mesh-stretching downstream of the combustor face is well-controlled. This is important to resolve the shear-layers exiting the venturi and for resolving the boundary layers at the walls.

2.2 RESULTS FOR 60^O SWIRLERS (LDI-1, 27ATM)

A steady-state RANS simulation was first performed for the LDI-1 configuration, for an upstream pressure of 27.6atm (P_3), T=811K (T_3). The inflow boundary condition for the CFD is set to a prescribed mass-flow rate that is computed from the experimental pressure drop (Δp=3% of P_3), effective area and air density. The exit boundary is set to a fixed static pressure equal to 97% of P_3.

The CFD solution is considered converged when the mass-flow imbalance between inflow and outflow boundaries drops (and stays) below 0.1% for 500 consecutive iterations. At convergence, the pressure predicted by the NCC code (at the inflow boundary) is used to compute the pressure drop across the single-element configuration. The pressure drop predicted by the NCC was within 10% of the measured experimental value of pressure drop.

The steady-state reacting computations proceeded from the steady-state non-reacting solutions in three steps:

1. Spray injection of fuel particles at a location 0.5mm downstream of the injector face. The spray parameters used were: 10 droplet groups, 60^o hollow cone (with 10^o thickness), 32 streams with stochastic injection. (See [Raju 2012] for more details of spray solver in the NCC code).
2. Ignition source terms were added downstream of each of the nine elements in a region 5-6mm downstream of the injector face to ignite the fuel-air mixture.
3. Reacting flow RANS computations were performed until the EINOx value at the exit plane converges.

The first finite-rate chemistry model used for RANS NCC included 14 species and 18 chemical reaction steps, with an 8-step NOx mechanism, as reported in [Ajmani, 2010]. Note that no attempt had been made to optimize for accurate NOx prediction in the kinetics used in this initial study. The consequence of this lack of NOx mechanism optimization can be seen in figure 2, in the relatively poor EINOx prediction when compared with the experimental data of [Tacina 2005].

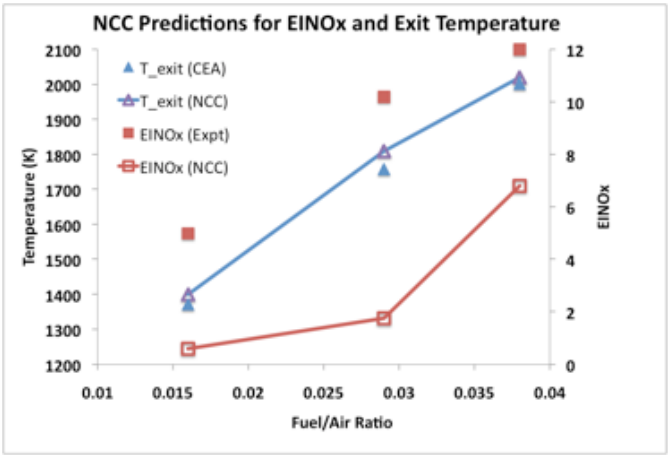

Figure 2: ϕ=0.24 (F/A=0.016), 0.43 (F/A=0.029) and 0.55 (F/A=0.038)NCC RANS predictions (non-optimized NOx mechanism) versus data [Tacina 2005]

The NCC RANS predictions with the *non-optimized* (for EINOx) reduced-kinetics mechanism, under-predicted EINOx for all three cases (ϕ=0.55, 0.43 and 0.24), particularly at ϕ=0.43 (Fuel/Air=0.029) and ϕ=0.24 (F/A=0.016). The average exit temperature (T_exit, NCC) at all three F/A ratios was within 20K-50K of the adiabatic equilibrium temperature (T_exit, CEA) from [Sanford 1994]. Detailed results of these NCC RANS computations (for a *nine*-element array with 60^o swirlers) were reported in [Ajmani 2013].

A reduced-kinetics mechanism *optimized* to match the emissions predictions of the detailed kinetics mechanism (JetSURF, [Sirjean 2009]) for Jet-A combustion was developed to attempt to improve the EINOx predictions with NCC RANS. The mechanism reduction was performed by modeling the LDI combustor as a well-stirred reactor (WSR) for the swirling flow near the dump plane, followed by a plug-flow reactor (PFR) for the well-mixed out region using [Chemkin 2013]. The optimization process focused on matching NOx produced by the reduced mechanism with that of the detailed mechanism, at a wide range of equivalence ratios (0.1<ϕ<1.5).

ϕ	T (Expt)	EINOx (Expt)	T (NCC)	EINOx (NCC)
0.25	1398	7.0	1387	2.8
0.39	1684	9.5	1744	7.3
0.43	1762	10.2	1784	8.3
0.56	1997	11.0	2070	13.5

Table 1: NCC prediction of T_4, EINOx for 60^o swirlers with *optimized* reduced-kinetics mechanism (P_3=27atm, T_3=811K

Table 1 shows NCC predictions for T_4 (exit temperature) and EINOx, as compared to experimental EINOx data and equilibrium temperature, obtained from NCC RANS computations on the *single*-element configuration shown in figure 1. The new, *optimized* reduced mechanism shows a dramatic improvement in the EINOx prediction for the LDI-1

60º configuration, as compared to the prediction with the non-optimized [Ajmani, 2010] mechanism (see figure 3).

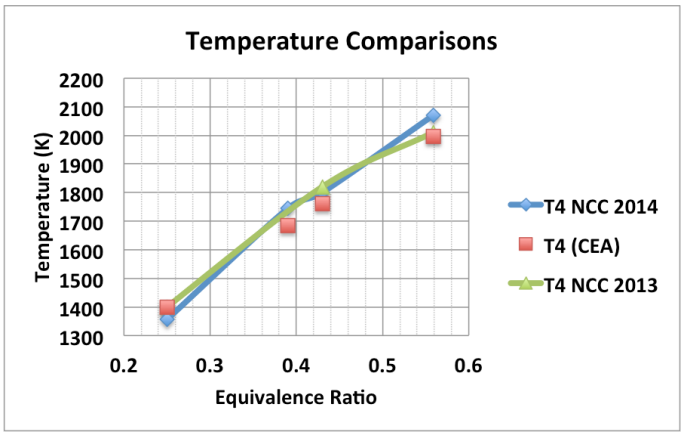

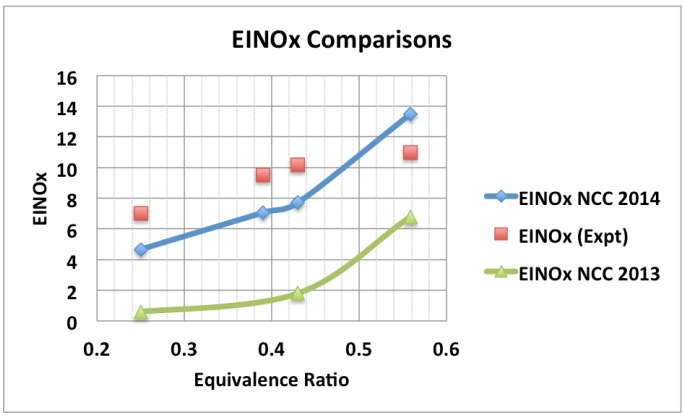

Figure 3: EINOx and Temperature (T_4) predictions for *non-optimized* (NCC 2013) and *EINOx optimized* (NCC 2014) reduced-kinetics mechanisms

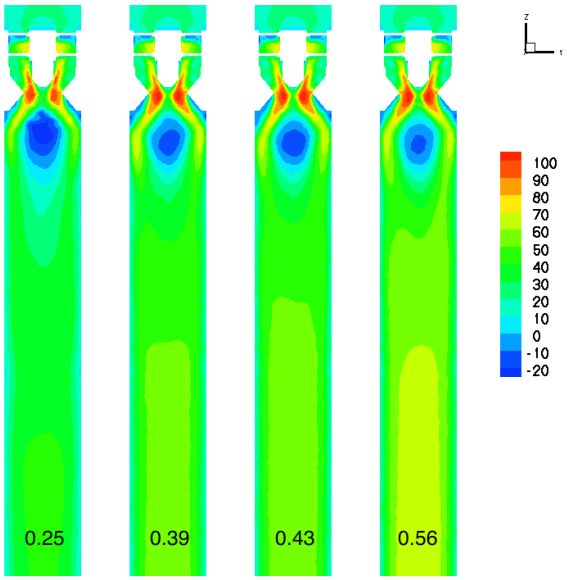

Figure 4: Axial-velocity (m/s) contours in Y=0 plane for ϕ=0.25, ϕ=0.39, ϕ=0.43 and ϕ=0.56 (left to right)

Figures 4-6 show axial-velocity, temperature, and EINOx contours for the steady-state RANS solution in an axial planes (Y=0) through the center of the LDI single-element configuration with 60º swirlers. The axial velocity contours show the presence of weak corner recirculation zones near the walls in the diverging section of the venturi, and strong detached primary recirculation zones downstream of the venturi exit plane (or the combustor dump plane). These flow features are typical of axial-swirlers with a 60º vane angle, as reported in the experimental data of [Fu 2009].

The strong but compact primary recirculation zone is responsible for the detached, compact flame downstream of the injector exit, as seen in figure 5. The diagnostic data of [Tacina 2014] seems to support the NCC RANS predictions of the flame structure. The NO mass-fraction contours in figure 6 show that NO formation is downstream of the primary burning zone for all cases, which is consistent with combustion theory.

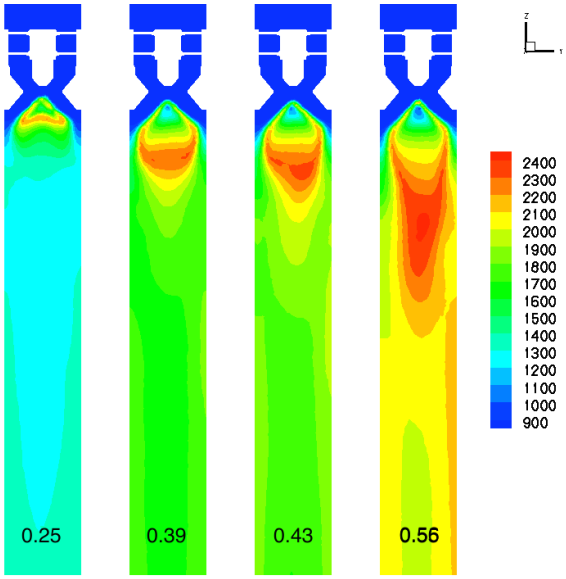

Figure 5: Temperature (K) contours in Y=0 plane for ϕ=0.25, ϕ=0.39, ϕ=0.43 and ϕ=0.56 (left to right)

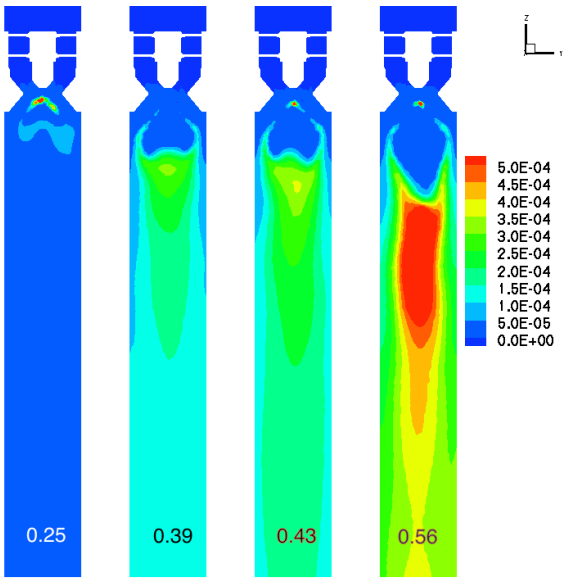

Figure 6: NO mass-fraction contours in Y=0 plane for ϕ=0.25, ϕ=0.39, ϕ=0.43 and ϕ=0.56 (left to right)

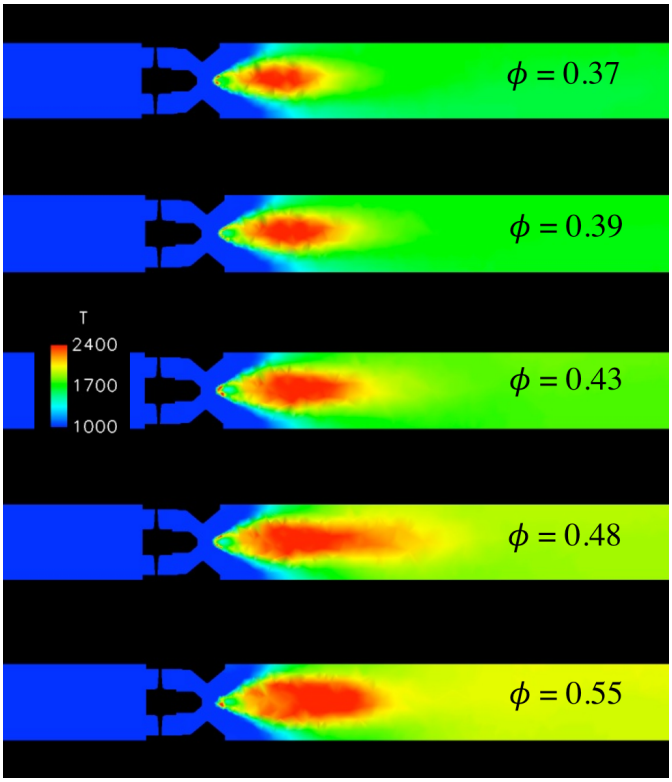

Figure 7. Temperature Contours for 45 degree swirler

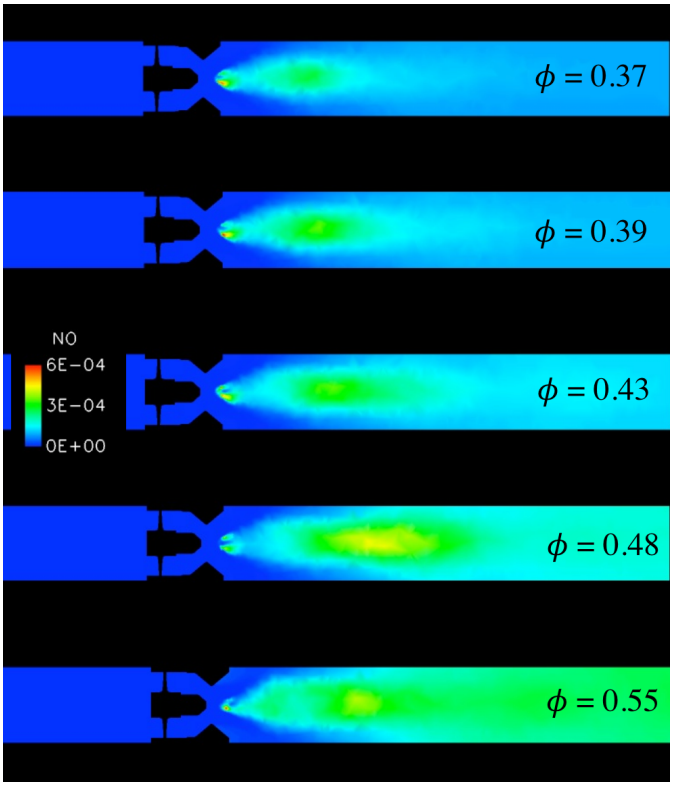

Figure 8. EINOx Contours for 45 degree swirler

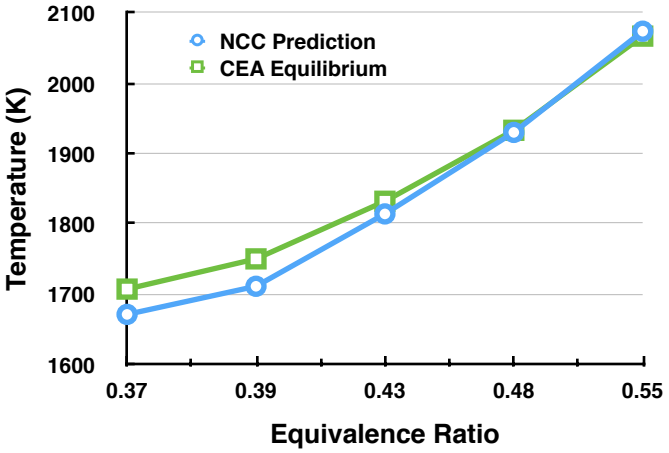

Figure 9. Temperature Comparisons for 45 degree swirler

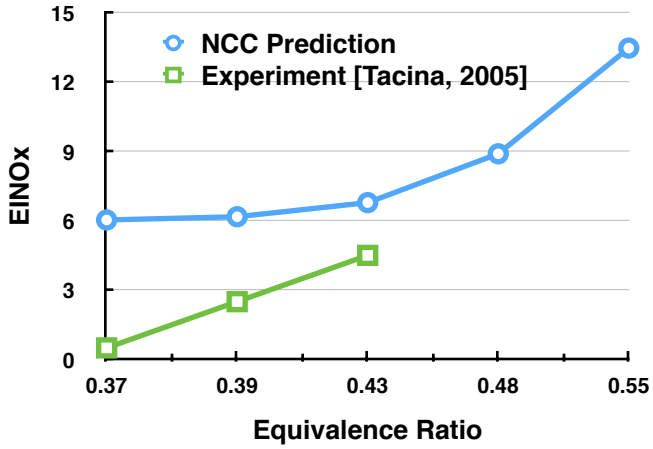

Figure 10. EINOx Comparisons for 45 degree swirler

2.3 RESULTS FOR 45^{O} SWIRLERS (LDI-1, 27ATM)

In order to study the effect of swirler vane-angle on performance and emissions, a steady-state RANS simulation was performed for a second LDI-1 configuration with 45^{o} helical vanes, for an upstream condition of 27.6atm (P_3), T=811K (T_3). The inflow boundary condition for the CFD was set to a prescribed mass-flow rate (0.1263kg/s) that was computed from the experimental pressure drop (Δp, 3% of P_3), effective area and air density. A fixed static pressure equal to P_3-Δp was set at the exit boundary.

Five different equivalence ratio conditions were computed with NCC RANS, with the aim of comparing predicted EINOx with available experimental data and comparing predicted T_4 with the equilibrium temperature computed from the CEA code. A tetrahedral mesh with 1.04M elements was generated, and the solution procedure with NCC RANS follows the (four step) staged computation procedure described earlier in this paper.

Temperature contours along an axial plane of the single-element injector are shown in figure 7. The size and intensity of the primary combustion zone increases as the equivalence ratio increases. In addition, the nature of the flame remains fairly consistent for all the computed equivalence ratios. Contours of NOx mass-fraction along an axial plane of the single-element injector are shown in figure 8.

Figure 9 shows a comparison of predicted T_4 temperature for five different computed equivalence ratios as compared to

the CEA equilibrium temperature. The NCC RANS predictions are in fairly good agreement with the CEA data for all the five computed cases. Figure 10 shows a comparison of predicted EINOx for five different computed equivalence ratios as compared to the available experimental data [Tacina, 2005]. The NCC RANS predictions for EINOx are in very poor agreement with the experimental data for all the five computed cases. The comparison of predicted EINOx at equivalence ratios below 0.43 is particularly poor, although the NCC RANS does predict the correct trend of increasing EINOx with equivalence ratio. The NOx produced increases in a non-linear fashion, particularly at equivalence ratios beyond 0.43.

2.4 RESULTS FOR 60^{O} SWIRLERS (LDI-1, 1ATM)

A second set of computational studies was performed with the 60^{o} swirler geometry, to evaluate the effects of single-step kinetics, multi-step reduced-kinetics, an Eulerian Monte-Carlo PDF method for turbulence chemistry interaction, in combination with RANS time-integration or the Time-Filtered Navier-Stokes (TFNS) integration model [Shih 2008] within the NCC. The set of computations described in this section were performed at P_3=1atm, T_3=293K, as extensive diagnostic data was available for comparison with NCC results.

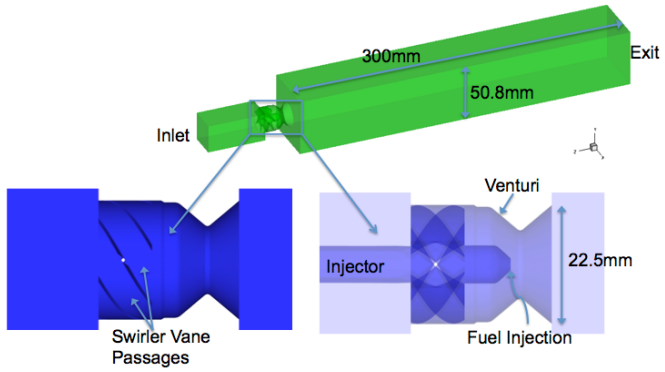

Figure 11: Single element LDI-I with 60-deg. vanes in a 2"x2" test section; reproduced from [Ajmani 2013].

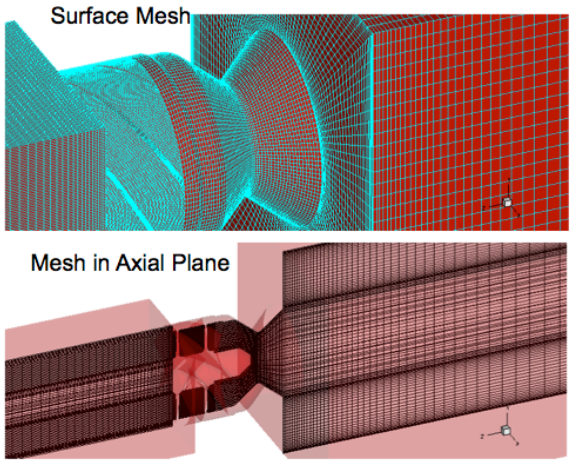

Figure 12: Surface mesh (top) and axial cross-section of mesh with. 1.26M hexahedral elements, obtained after two mesh iterations with 0.9M and 1.1M elements

Figure 11 shows the computational setup for a single element LDI-1 configuration with 60^{o} helical vanes. The setup is very similar to that described in section 2.2, except that the downstream section is 4x larger in area, to mimic the experimental setup. The portion of the mesh corresponding to the computational setup is shown in figure 12, with the surface mesh (top), and an axial-plane cross-section (bottom) of the fully-hexahedral mesh of 1.26M elements.

2.4.1 NCC TFNS WITH MONTE-CARLO PDF

The effect of turbulent-chemistry interaction on the single-element, reacting-flow predictions, was studied by replacing laminar chemistry with a joint scalar monte-carlo PDF model. In this approach, the velocity and turbulence fields are solved using a conventional CFD solver, a modeled PDF transport equation provides the solution for the species and temperature fields, and a lagrangian spray formulation is used for the liquid-phase. The Monte Carlo method is used for solving the PDF equation because the computational effort increases only linearly with the increase in the dimensionality of the PDF transport equation [Raju 2004].

Figures 13 and 14 show comparisons of axial-velocity and temperature for four reacting-flow modeling approaches: RANS and TFNS with single-step kinetics and laminar chemistry, TFNS with multi-step kinetics and laminar chemistry, and TFNS with multi-step kinetics and turbulence-chemistry interaction (Monte-Carlo PDF). The axial-velocity and temperature contours show significant differences for the four approaches.

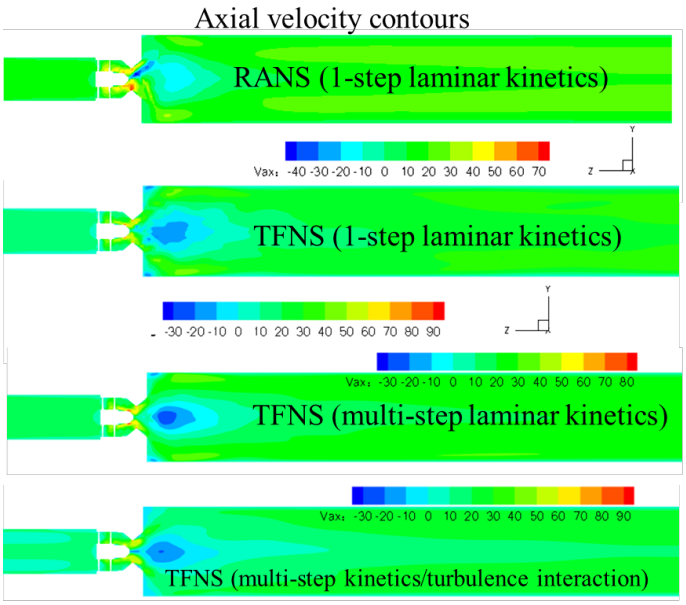

Figure 13: Axial velocity contours of the single element 60^{o} LDI axial-velocity (m/s) affected by the four selected simulation models, viz. RANS and TFNS with laminar kinetics involving single-step and multi-steps and turbulence/chemistry interaction (P_3=1atm, T_3=293K, ϕ=0.75, Δp=4%)

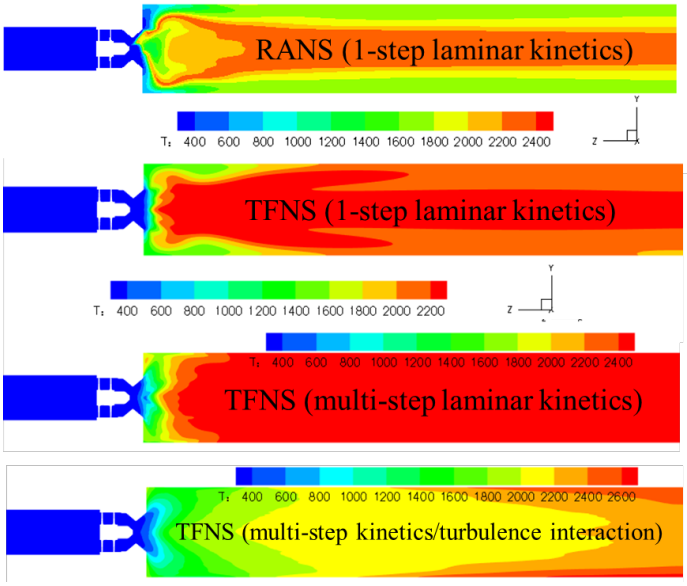

Figure 14: Temperature contours of the single element 60º LDI axial-velocity (m/s) affected by the four selected simulation models, viz. RANS and TFNS with laminar kinetics involving single-step and multi-steps and turbulence/chemistry interaction.

A centerline comparison of axial-velocity and temperature for TFNS (with and without Monte-Carlo PDF), with the experimental data of [Cai 2005] is shown in figure 15. The inclusion of Monte-Carlo PDF turbulence-chemistry interaction significantly improves the NCC TFNS prediction of centerline temperature, when compared with experimental data.

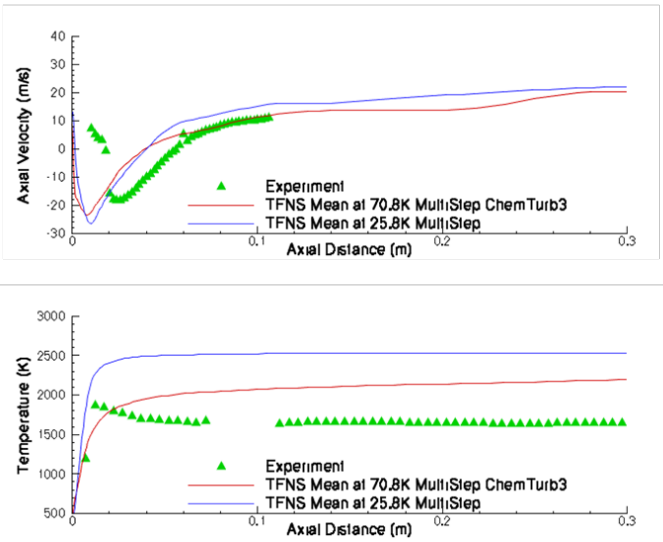

Figure 15: The measured profiles of centerline axial velocity (m/s) and temperature (K) [Cai 2005] compared with the multi-step TFNS predictions assuming laminar kinetics (blue line) and turbulence-chemistry interaction shown as red line.

Figure 16 summarizes the final solution (time-averaged quantities) for NCC TFNS with Monte-Carlo PDF and multi-step reduced chemical kinetics. Contours of axial-velocity, temperature, OH mass-fraction and CO mass-fraction are shown, in order to provide insights into the mixing characteristics and flame development of this 60º single-element LDI-1 configuration.

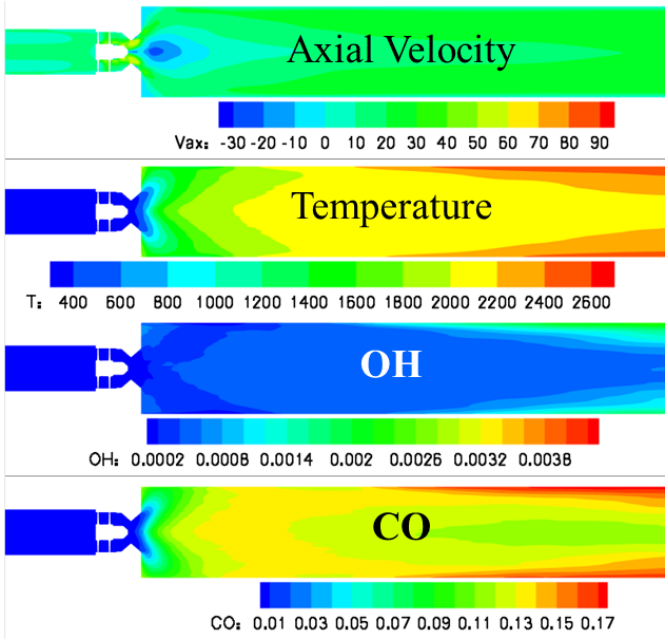

Figure 16: Contours of axial velocity, temperature, OH and CO of the single element 60º LDI predicted by multi-step TFNS with turbulence/chemistry interaction

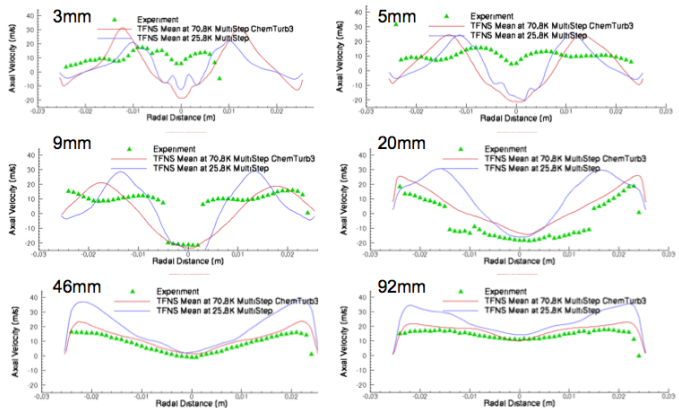

Figure 17: The measured profiles of axial velocity (m/s) [Cai 2005] compared with the multi-step kinetics TFNS predictions assuming laminar chemistry (blue line) and turbulence/ chemistry interaction (red line).

A detailed comparison of axial-velocity and temperature predictions from NCC TFNS (with and without Monte-Carlo PDF), at different axial locations downstream of the combustor dump plane, is shown in figures 17 and 18, respectively. The axial velocity predictions, with or without turbulence-chemistry interaction, at 3mm and 5mm are poor, particularly near the centerline. However, the inclusion of turbulence-chemistry interaction does improve the axial velocity predictions at the four downstream locations of 9mm, 20mm, 46mm and 92mm. The temperature predictions of NCC TFNS also benefit from the inclusion of turbulence-chemistry interaction, as seen in the comparisons at the four downstream locations of 20mm, 30mm,

67mm and 150mm. In summary, the inclusion of Monte-Carlo PDF turbulence-chemistry interaction significantly improves the NCC TFNS predictions, when used with the multi-step reduced kinetics mechanism approach studied in this paper.

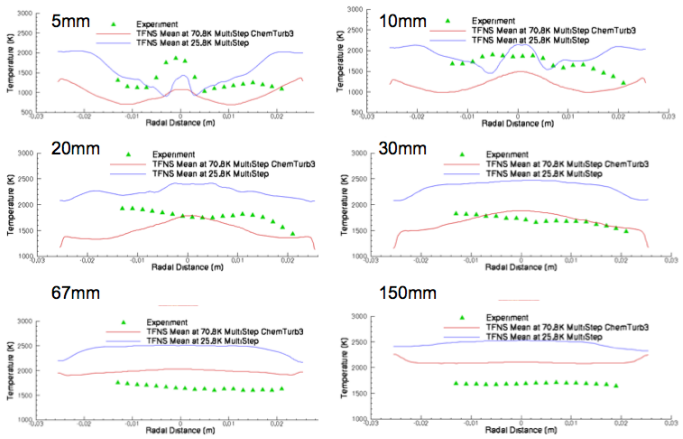

Figure 18: The measured profiles of Temperature (K) [Cai 2005] compared with the multi-step kinetics TFNS predictions assuming laminar chemistry (blue line) and turbulence/ chemistry interaction (red line).

3.0 CONCLUSIONS AND FUTURE WORK

The National Combustion Code (NCC) was successfully used to perform reacting-flow RANS computations on two different single-element LDI-1 injectors with bladed-swirler configurations. A new, reduced kinetics-mechanism, *optimized* for emissions predictions at 2.76MPa conditions, considerably improved the EINOx predictions for a 60º bladed-swirler LDI-1 configuration, when compared with a previous, *non-optimized* reduced-kinetics model. An additional assessment of a second reduced-kinetics mechanism optimized for 0.1MPa conditions, also showed great promise in improving axial-velocity and temperature predictions, when assessed with NCC TFNS and a turbulence-chemistry interaction (Monte-Carlo PDF) model.

In future work, detailed comparisons of experimental emissions data (CO, NOx) for the 0.1MPa LDI-1 configuration, with NCC TFNS and updated turbulence-chemistry interaction models [Liu 2014] will be performed. In addition, efforts will also focus on application of the reduced kinetics-mechanism assessed in this paper, for emissions predictions of *multiple* element, next-generation LDI-2 and LDI-3 candidate designs using NCC TFNS. The stated goal is to use a computational tool like NCC TFNS (with turbulence-chemistry interaction and reduced-kinetics mechanisms) to positively impact the design cycle of LDI-2 and LDI-3 combustors.

4.0 REFERENCES

[Ajmani, 2010] Ajmani, K., Kundu, K. P. and Penko, P., "A Study on Detonation of Jet-A Using a Reduced Mechanism", 48th AIAA Aerospace Sciences Meeting, Orlando FL, AIAA Paper 2010-1515

[Ajmani, 2013] Ajmani, K., Mongia, H., and Lee, P., "CFD Best Practices to Predict NOx, CO and Lean Blowout for Combustor Design", Proceedings of ASME Turbo Expo 2013, GT 2013-95669.

[Ajmani, 2014a] Ajmani, K., Mongia, H., and Lee, P., "CFD computations of emissions for LDI-2 combust ors with simplex and airblast injectors", AIAA Paper 2014-3529, 50th AIAA Joint Propulsion Conference, July 2014.

[Ajmani, 2014b] Ajmani, K., and Breisacher, K., "Simulations of NOx Emissions from Low Emissions Discrete Jet Injector Combustor Tests", AIAA Paper 2014-3524, 50th AIAA Joint Propulsion Conference, July 2014.

[Cai, 2005] Cai, J., Jeng, S.-M., and Tacina, R., "The Structure of a Swirl-Stabilized Reacting Spray Issued from an Axial Swirler," AIAA Paper 2005-1424.

[Chemkin, 2013] CHEMKIN-PRO 15131, Reaction Design, San Diego, 2013.

[Fu, 2008] Fu, Y., "Aerodynamics and Combustion of Axial Swirlers", PhD Thesis, University of Cincinnati, 2008.

[Gokulakrishnan, 2013] Gokulakrishnan, P., Joklik, R., Viehe, D., Trettel, A., Gonzalez-Juez, E., and Klassen, M., "Optimization of Reduced Kinetic Models for Reactive Flow Simulations," GT2013-95215, Proceedings of ASME Turbo Expo 2013, San Antonio, Texas.

[Iannetti 2008] Iannetti, A., Liu, N.-S., Davoudzadeh, H. "The Effect of Spray Initial Conditions on Heat Release and Emissions in LDI CFD Calculations", NASA/TM 2008-215422, NASA Glenn Research Center.

[Lee 2013] Lee, C.-M., Chang, C., Kramer, S., and Hebron, J.T., "NASA Project develops next generation low-emission Combustor Technologies," 51st AIAA Aerospace Sciences Meeting, Dallas TX, AIAA Paper 2013-0540.

[Liu 2007] Liu, N.-S., Shih, T.-H., and Wey, C.T., "Comprehensive Combustion Modeling and Simulation: Recent Progress at NASA Glenn Research Center," ISABE-2007-1268, 18th International Symposium on Air Breathing Engines, September 2-7, 2007, Beijing, China.

[Liu 2011] Liu, N.-S., Shih, T.-H., and Wey, C.T., "Numerical Simulations of Two-Phase Reacting Flow in a Single- Element Lean Direct Injection (LDI) Combustor Using NCC", NASA/ TM 2011-217031, NASA Glenn Research Center.

[Liu 2014] Liu, N.-S. and Wey, C.T., "On The TFNS Sub-Grid Models for Liquid-Fueled Turbulent Combustion," AIAA Paper 2014-3569, 50th AIAA Joint Propulsion Conference, July 2014.

[Mongia 2008] Mongia, H. C., 2008, "Recent Progress in Comprehensive Modeling of Gas Turbine Combustion," AIAA Paper 2008-1445.

[Raju 2004] Raju, M.S., "Current Status of the Overall Spray Solution Procedure (Combined CFD/Scalar- Monte-Carlo-PDF/

Spray Computations) developed under NCC," AIAA–2004–0327, 42nd AIAA Aerospace Sciences Meeting and Exhibit, January 2004.

[Raju 2012] Raju, M. S., "LSPRAY-IV: A Langrangian Spray Module," NASA CR-2012-217294.

[Sanford, 1994] Sanford, G., and McBride, B., "Computer program for calculation of complex chemical equilibrium compositions and applications. Part 1: Analysis", NASA-RP-1311, 1994.

[Shih 2003] Shih, T.-H., Povinelli, L. A., and Liu, N.-S., "Application of Generalized Wall Function for Complex Turbulent Flows," Journal of Turbulence, Vol. 4, April 2003, pp 1.-16.

[Shih 2008] Shih, T.-H., Liu, Nan-Suey Assessment of the Partially Resolved Numerical Simulation (PRNS) Approach in the National Combustion Code (NCC) for Turbulent Nonreacting and Reacting Flows, NASA TM 2008-215418.

[Sirjean 2009] Sirjean, Dames E, Sheen DA, Egolfopoulos FN, Wang H, Davidson DF, Hanson RK, Pitsch H, Bowman CT, Law CK, Tsang W, Cernansky NP, Miller DL, Violi A, Lindstedt RP., "A high-temperature chemical kinetic model of n-alkane, cyclohexane, and methyl-, ethyl-, n-propyl and n-butyl-cyclohexane oxidation at high temperatures", (JetSurF version 1.1) 2009 Sep 15; http://melchior.usc.edu/JetSurF/JetSurF1.1.

[Tacina 2005] Tacina, R., Lee, P. and Wey, C., "A Lean-Direct-Injection Combustor Using a 9 Point Swirl-Venturi Fuel Injector", ISABE Conference 2005, Paper 2005-1106.

[Tacina 2014] Tacina, K.M., Hicks, Y.R., and Tedder, S.A., "Fundamental Study of a Single-Point Lean Direct Injector. Part III: Unsteady Effects," Paper 089IC-0051, 2014 Technical Meeting of the Central States Section of the Combustion Institute, March 2014.

ACKNOWLEDGEMENTS

This work was funded in part by NASA Glenn Research Center (GRC) under the Environmentally Responsible (ERA) project. The authors are grateful to NASA's NAS Supercomputing facility for computational resources.

APPENDIX A

A reduced chemical kinetics mechanism was optimized for emissions computations of Jet-A/Air combustion in Lean Direct Injection (LDI) combustors. The kinetics model uses **A** (pre-exponential factor), **n** (temperature exponent) and **E** (activation energy, cal/mol) to compute the Arrhenius rate coefficient, $\mathbf{k = A\,(T/T_0)^n\,e^{(-E/RT)}}$, for a given temperature, **T** (K). (**R** = universal gas constant, $\mathbf{T_0}$ (K) is a reference temperature).

Reduced Kinetics Mechanism Optimization for P3=27atm

A 14-species, 19-step reduced mechanism was optimized for combustion of Jet-A/Air at high-pressure conditions of 27atm (2.76MPa). An optimization was performed to match heat release (T4) and emissions profiles (NO, CO) of the reduced mechanism with the JetSURF [Sirjean 2009] detailed mechanism, for Jet-A/Air combustion. The results of the optimization for T4 (equilibrium temperature), NO and CO, are shown in Figures A.1, A.2, and A.3, respectively. The *optimized* reduced mechanism which was implemented in the NCC, and assessed with RANS computations for two different Lean Direct Injection (LDI) configurations (see sections 2.2 and 2.3), is shown in Table A.1

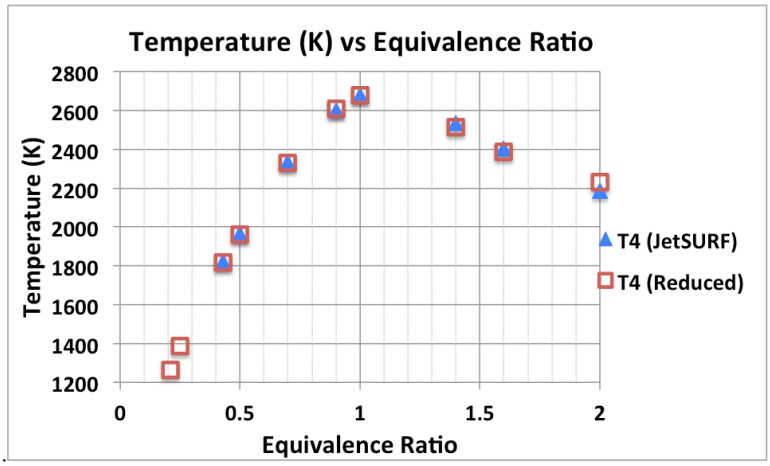

Figure A.1 Equilibrium temperature (T4) computed with [Chemkin 2013] for Jet-A/Air combustion - JetSURF [Sirjean 2009] detailed chemistry versus 'reduced' chemistry (current work)

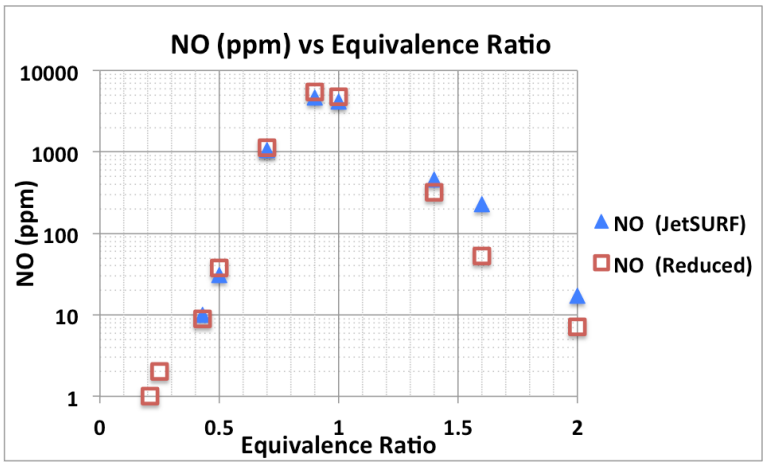

Figure A.2 NO mole-fraction computed with [Chemkin 2013] for Jet-A/Air combustion - JetSURF [Sirjean 2009] detailed chemistry versus 'reduced' chemistry (current work)

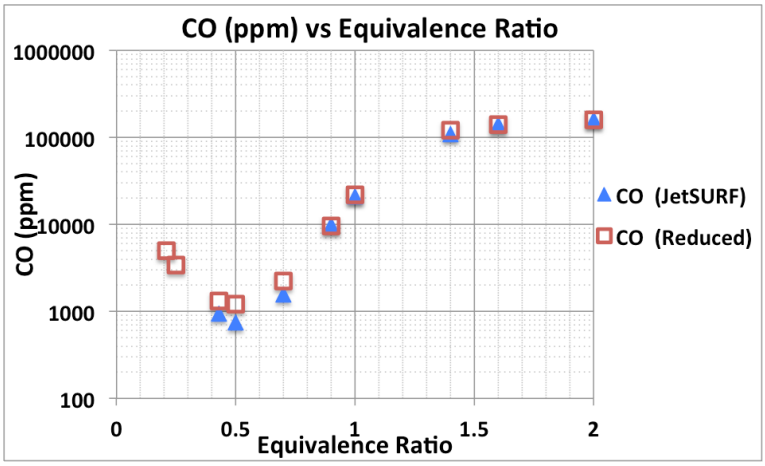

Figure A.3 CO mole-fraction computed with [Chemkin 2013] for Jet-A/Air combustion - JetSURF [Sirjean 2009] detailed chemistry versus 'reduced' chemistry (current work)

14 Species, 19 Step Optimized Mechanism (27atm)

	Reaction	A	n	E
1	C11H21 + O2 => 11CH + 10H + O2	3.00E+13	0.00	3.1E+04
	GLO / C11H21 0.8 / GLO / O2 0.9 /			
2	CH + O2 => CO + OH	3.00E+11	0.00	0.0
3	CH + O => CO + H	3.00E+12	1.00	0.0
4	H2 + O2 <=> H2O + O	3.98E+11	2.00	2.8E+04
5	H2 + O <=> H + OH	3.00E+14	0.00	6.00E+03
6	H + O2 <=> O + OH	4.00E+14	0.00	1.80E+04
7	CO + OH + O <=> CO2 + H + O	2.52E+13	1.85	-2.58E+02
8	CO2 + H <=> CO + OH	2.14E+12	0.80	2.59E+04
9	H2O + O2 <=> 2O + H2O	2.57E+16	0.00	1.12E+05
10	CO + H2O + H2 <=> CO2 + 2H2	5.00E+08	1.48	-1.00E+03
11	CO + H2 + O2 <=> CO2 + H2O	1.30E+10	1.60	-1.00E+03
12	N + O2 <=> NO + O	1.50E+07	1.20	1.00E+04
13	N + OH <=> NO + H	5.00E+12	1.40	4.8E+04
14	NO + C11H21 <=> N + O2 + C11H21	3.00E+16	1.0	0.0
15	H + N2O <=> N2 + OH	1.00E+17	0.00	7.55E+02
16	N2 + O2 + O <=> N2O + O2	2.00E+15	0.00	3.02E+02
17	N2 + H2 + O <=> N + NO + H2	1.00E+16	0.20	3.02E+02
18	N2O + O <=> 2NO	1.50E+15	0.00	4.80E+04
19	N2O + N2 <=> 2N2 + O	1.00E+13	0.10	0.0

Table A.1 *Optimized* Reduced Mechanism Assessed with NCC RANS for two LDI configurations at P_3=27atm

Reduced Kinetics Mechanism Optimization for P3=1atm

A second, 14-species, 21-step reduced mechanism was optimized for combustion of Jet-A/Air at *atmospheric*-pressure conditions of 1atm (0.1MPa), and is shown in Table A.2. In order to save computational time when assessing the reduced model with NCC TFNS and a Monte-Carlo PDF turbulent-chemistry interaction model, only the first ten steps of the mechanism were used to compare flow characteristics like axial-velocity and temperature with detailed experimental data (see section 2.4). Future computations will include the additional 11-step NO mechanism of Table A.2, and compare NO and CO emissions predictions of NCC TFNS with available experimental data.

14-Species, 21-Step Optimized Mechanism (1atm)

	Reaction	A	n	E
1	C11H21 + N2 => 11CH + 10H + N2	3E+12	0.00	3.1E+04
	GLO / C11H21 0.8 / GLO / N2 0.8 /			
2	CH + O2 => CO + OH	2.00E+15	0.00	0.0
3	CH + O => CO + H	3.00E+12	1.00	0.00E+00
4	H2 + O2 <=> H2O + O	3.98E+10	1.00	2.8E+04
5	H2 + O <=> H + OH	3.00E+14	0.00	6.00E+03
6	H + O2 <=> O + OH	4.00E+14	0.00	1.80E+04
7	CO + OH <=> CO2 + H	4.01E+06	1.25	-7.58E+02
8	H2O + O2 <=> 2O + H2O	2.71E+15	1.85	1.12E+05
9	CO + H2O <=> CO2 + H2	2.7E+08	1.28	-1.00E+03
10	CO + H2 + O2 <=> CO2 + H2O	6.0E+11	1.60	1.80E+04
11	N + O2 <=> NO + O	7.0E+06	1.00	3.17E+03
12	O + NO <=> N + O2	1.4E+13	0.00	4.17E+04
13	N + OH <=> NO + H	1.0E+12	1.25	3.80E+04
14	N + N + M <=> N2 + M	6.67E+19	3.6	7.3E+04
15	NO + C11H21 <=> N + O + C11H21	4.00E+09	0.00	0.0
16	H + N2O <=> N2 + OH	1.5E+14	0.00	7.55E+02
17	N2 + O <=> N + NO	4.75E+13	0.10	7.50E+04
18	N2 + O2 + O <=> N2O + O2	1.0E+19	0.00	3.02E+02
19	N2 + H2 + O <=> N + NO + H2	1.0E+15	0.10	3.02E+02
20	N2O + O <=> 2NO	1.50E+15	0.00	4.80E+04
21	N2O + N2 <=> 2N2 + O	2.96E+16	0.00	3.32E+04

Table A.2 *Optimized* Reduced Mechanism Assessed with NCC TFNS for an LDI configuration at P_3=1atm